magnetochemistry

MDPI

Article

Manganese (III) Compounds Derived from R-Salicylaldoxime and 9-Anthracenecarboxylate Ligands: A Study of Their Synthesis and Structural, Magnetic, and Luminescent Properties †

Berta Casanovas [1], Ramon Vicente [1], Mercè Font-Bardía [2] and Mohamed Salah El Fallah [1,*]

[1] Departament de Química Inorgànica i Orgànica, Secció de Química Inorgànica and Institut de Nanociència i Nanotecnologia (IN2UB), Universitat de Barcelona, Martí i Franquès 1-11, 08028 Barcelona, Spain
[2] Departament de Mineralogia, Cristal·lografia i Dipòsits Minerals and Unitat de Difracció de RX. Centre Científic i Tecnològic de la Universitat de Barcelona (CCiTUB), Universitat de Barcelona, C/Solé i Sabarís, 1-3, 08028 Barcelona, Spain
* Correspondence: salah.elfallah@qi.ub.es; Tel.: +34-93-4039134

† During the preparation of this manuscript dedicated to Professors Miguel Julve and Francesco Lloret on the occasion of their retirements, and before submitting it to the Magnetochemistry journal, we received the sad news of the death of one of the honourees, Prof. Miguel Julve. We deeply regret the loss of one of the most distinguished professors in the field of coordination chemistry, especially in the area of molecular magnetism. We regret the loss of a great friend, a big communicator, and a giant scientist. Miguel, we will miss you, but you will live in our memory with the beautiful moments shared with you. Thank you for your friendship, humility and availability. "Descansa en paz Miguel".

Abstract: The reaction of Mn(II) salts in the air with different R-salicylaldehyde oximes and the sodium or cesium salts of 9-anthracenecarboxylato (9-AC) allows for the isolation of new six polynuclear compounds: $[Mn_3NaO(salox)_3(9\text{-}AC)_2(EtOH)_3H_2O]_n \cdot 2EtOH$ (**1**), $[Mn_3NaO(3\text{-}Me\text{-}salox)_3(9\text{-}AC)_2(EtOH)_3H_2O]_n \cdot EtOH$ (**2**), $[Mn_6O_2(salox)_6(9\text{-}AC)_2(EtOH)_2(H_2O)_2] \cdot 3EtOH$ (**3**), $[Mn_3O(3\text{-}Me\text{-}salox)_3(9\text{-}AC)(EtOH)_3(H_2O)] \cdot 1.8EtOH \cdot 3H_2O$ (**4**), $[Mn_6O_2(Me\text{-}salox)_6(9\text{-}AC)_2(EtOH)_4(H_2O)_2] \cdot 0.5H_2O$ (**5**), and $[Mn_6O_2(Et\text{-}salox)_6(9\text{-}AC)_2(EtOH)_4(H_2O)_2] \cdot 3EtOH$ (**6**). H_2salox is a salicylaldehyde oxime, H_2(3-Me-salox) is a 3-methyl-salicylaldehyde oxime, H_2Me-salox is a 1-(2-hydroxyphenyl)ethan-1-one oxime and a H_2-Et-salox is 1-(2-hydroxyphenyl)propan-1-one oxime. Structurally, compounds **1** and **2** consist of chains of trinuclear $\{Mn^{III}_3(\mu_3\text{-}O)(salox)_3\}^+$ units connected by Na^+ ions. Compounds **3**, **5**, and **6** are hexanuclear units formed by two parallel trinuclear units $\{Mn^{III}_3(\mu_3\text{-}O)(salox)_3\}^+$ or $\{Mn^{III}_3(\mu_3\text{-}O)(Me\text{-}salox)_3\}^+$ planes related through an inversion center. Compound **4** consists of two isolated $[Mn_3O(3\text{-}Me\text{-}salox)_3(9\text{-}AC)(EtOH)_3(H_2O)]$ trinuclear molecules in the unit cell showing crystallographic differences. Magnetic studies reveal a set of antiferromagnetic interactions in compounds **1** and **2** and a combination of antiferromagnetic and ferromagnetic interactions in compounds **3**, **5**, and **6**. In all cases, the magneto-structural correlation between the intramolecular Mn^{III}-N-O-Mn^{III} torsion angle and the magnetic exchange within these units have been confirmed. For compounds **5** and **6**, *ac* magnetic measurements reveal the slow relaxation of magnetization with moderate energy barriers of 19.9 cm^{-1} and 31.1 cm^{-1}, respectively. Absorbance and fluorescence measurements in solution show the transitions of the 9-anthracenecarboxylate chromophore for all the compounds.

Keywords: manganese coordination compounds; magnetic properties; single-molecule magnets; luminescence

check for updates

Citation: Casanovas, B.; Vicente, R.; Font-Bardía, M.; El Fallah, M.S. Manganese (III) Compounds Derived from R-Salicylaldoxime and 9-Anthracenecarboxylate Ligands: A Study of Their Synthesis and Structural, Magnetic, and Luminescent Properties. *Magnetochemistry* **2024**, *10*, 55. https://doi.org/10.3390/magnetochemistry10080055

Academic Editors: Carlos J. Gómez García and Salah-Eddine Stiriba

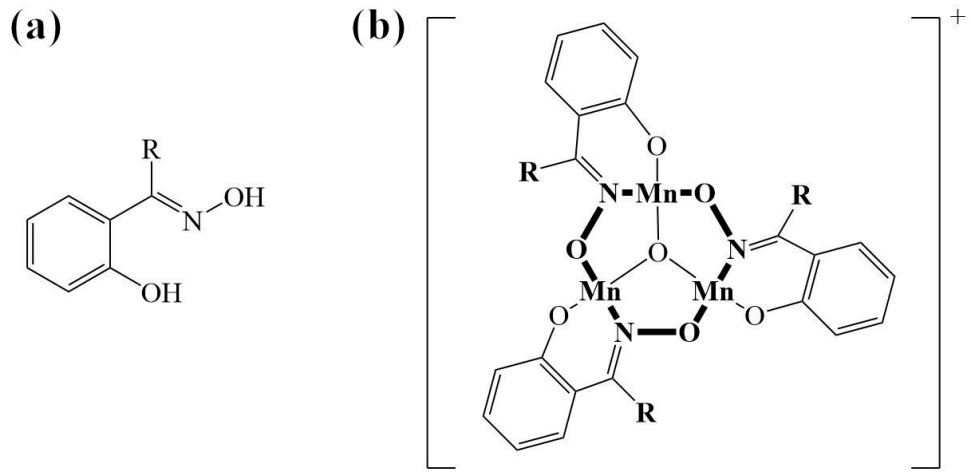
Received: 15 July 2024
Revised: 31 July 2024
Accepted: 3 August 2024
Published: 5 August 2024

Copyright: © 2024 by the authors. Licensee MDPI, Basel, Switzerland. This article is an open access article distributed under the terms and conditions of the Creative Commons Attribution (CC BY) license (https://creativecommons.org/licenses/by/4.0/).

1. Introduction

At the beginning of the year 2000, our research group described two new hexanuclear compounds with the formulas of $[Mn_6O_2(salox)_6(Me\text{-}COO)_2(EtOH)_4]$ and $[Mn_6O_2(salox)_6(Ph\text{-}COO)_2(EtOH)_4]$ [1]. These compounds are constructed by two triangular entities $\{Mn^{III}_3(\mu_3\text{-}O)\ (salox)_3\}^+$, where $salox^{2-}$ is the anion derived from the double deprotonation of the salicylaldoxime ligand represented in Scheme 1a. These kinds of ligands are

commonly used for metal extraction or as anticorrosive agents in coating processes [2]. The structure of the trinuclear unit represented in Scheme 1b consists of three Mn(III) ions connected by a μ_3-O^{2-} anion, located at the center of the triangle, and by the nitrogen and oxygen atoms of the oxime groups of three R-salox^{2-} ligands, which bridge each pair of Mn(III) ions. These ligands also coordinate terminally with each of the Mn(III) ions through the oxygen in the phenolate group. Numerous research groups call these compounds "inverse metallacrowns" because they feature a cyclic M-N-O repeat unit and contain an anion in the central cavity [3–6]. Due to the extensive synthetic possibilities arising from the use of different substituted salicylaldoximes, H_2-R-salox (R = H, CH_3 (Me), CH_3CH_2 (Et)...) [7–10], as well as the types of counterions or used solvents, many compounds based on the same trinuclear group $\{Mn^{III}_3(\mu_3\text{-}O)(\text{R-salox})_3\}^+$ have been obtained. The most used counterions are carboxylates and azide anions. Generally, in these compounds, Mn(III) ions exhibit either an octahedral coordination geometry with Jahn–Teller distortions or a square pyramidal type. In both cases, the equatorial or basal positions lie in the same $[Mn_3]$ plane. Magnetic studies revealed that hexanuclear compounds exhibit a ground spin state of S = 4, derived from the ferromagnetic coupling between the two trinuclear units with S = 2, resulting from the intra-triangular antiferromagnetic coupling among the three high-spin Mn(III) ions ($S_{Mn(III)}$ = 2). Furthermore, it was observed that these compounds exhibit single-molecule magnet (SMM) behavior [1].



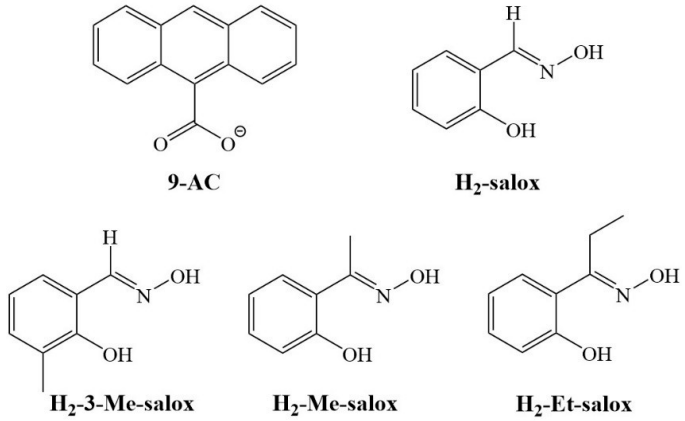
Scheme 1. (**a**) General representation of the H_2-R-salicylaldoxime ligands. (**b**) Trinuclear entity $\{Mn^{III}_3(\mu_3\text{-}O)(\text{R-salox})_3\}^+$.

Several systematic studies on hexanuclear compounds with R-salox^{2-} ligands having different alkyl groups and carboxylate ligands varying in size have corroborated that by increasing the volume of the R group in the substituted salox^{2-} anions, the fundamental spin state can increase from S = 2 to S = 12, which is the maximum possible value for this kind of hexanuclear system as a consequence of the ferromagnetic coupling between all Mn(III) ions [11]. Subsequently, through a detailed observation of the structure and the magnetic properties of different hexanuclear systems, it was postulated that the generally weak coupling [12] between Mn(III) ions within the triangle is mainly dominated by the Mn–N–O–Mn torsion angle. A so-called "magic area" is present when this angle ranges between 30.4° and 31.3° [13]. According to the established magneto-structural correlation, if the angles are below 30.4°, antiferromagnetic coupling ($J < 0$) is expected, while torsions greater than 31.3° are expected to result in ferromagnetic exchange ($J > 0$). If the torsion angle falls within this range, the magnetic exchange between the ions can be either antiferromagnetic or ferromagnetic. The Mn–N–O–Mn torsion angle increases as the volume of R-substituent groups of the oxime group increases. The fundamental spin state of the triangle is determined by the contribution of each of the three couplings via the oxime group, and thus, taking the average value of the torsion angles is not valid. In all

cases, it was observed that the coupling between triangles via the R-salox^{2-} ligands is of a ferromagnetic nature. Moreover, when all the magnetic exchanges between Mn(III) ions are ferromagnetic, the larger the torsion angles, the higher the magnetization relaxation barrier. This experimental fact is attributed to an increase in the coupling constant, *J*, which results in the ground state, S, being more energetically isolated from the excited states, thus preventing tunneling relaxation [10]. In these triangular units, the anisotropy axes of Mn(III) are almost parallel and perpendicular to the $[Mn^{III}]_3$ triangular planes, resulting in the formation of compounds, with *d* metals exhibiting the highest observed magnetization energy barrier [14]. The dominance of the Mn-N-O-Mn torsion angle value over the coupling between Mn(III) atoms observed in published hexanuclear compounds is valid for any compound containing triangular units $\{Mn^{III}_3(\mu_3\text{-O})(Rsalox)_3\}^+$ [15]. Within each triangular unit, depending on the torsion angles present in the compound, the total spin (S) can range from 0 to 6.

The compounds based on $\{Mn^{III}_3(\mu_3\text{-O})(R\text{-salox})_3\}^+$ units and carboxylate anions generally have the general formula $[Mn^{III}_xO_{1\text{-}2}$ (R-salox)$_x$(R-COO)$_{1\text{-}2}$(L)$_{4\text{-}6}]$, where R = H, CH_3 (Me), CH_2CH_3 (Et), C_6H_5 (Ph)... [1,8–11,16], L = solvent (alcohols or water), and x = 3 or 6 [7]. In some instances, the use of poly-carboxylates has led to the formation of 1D or even 2D compounds based on the same unit core [17,18].

On the other hand, it is well known that the anthracene aromatic group of the carboxylate ligand shows luminescent properties [19] that can be maintained when the ligand is complexed, as has been observed in different manganese coordination compounds with different ligands that contain anthracene groups [20–23]. Therefore, the aim of this work is obtaining multifunctional compounds based on the $\{Mn^{III}_3(\mu_3\text{-O})(Rsalox)_3\}^+$ unit that exhibit interesting magnetic properties and anthracenecarboxylate ligands, where the presence of the π-conjugated system could offer luminescence properties to the Mn compounds. We also aimed to investigate how different cations (Na^+ or Cs^+) in alkaline carboxylate salt and the anion of the starting manganese salt (NO_3^- or ClO_4^-) influence the structure and, consequently, the magnetic and luminescent properties of the new compounds. The incorporation of Na^+ ions in the synthesis of compounds featuring the $\{Mn^{III}_3(\mu_3\text{-O})(R\text{-salox})_3\}^+$ unit and carboxylate ligands has been previously explored to achieve new topologies. It has been observed that this cation can serve as a linkage point between $[Mn_3]$-based units, forming several structural architectures, such as dimers of trinuclear units [15,24], $[Mn_{18}]$ [25], as well as 1D [26,27] or 2D structures [28–30]. In all the compounds, Na^+ ions present a hexacoordinated environment, and it is observed that the alkaline cations keep the Mn(III) units well-isolated. As a result, their binding does not affect the intra-triangular magnetic properties. Additionally, we decided to investigate the effect of other alkaline ions with a larger ionic radius than Na^+, such as Cs^+, a variable that has not been explored to date. Also, we examine the effect of the substitution of hydrogen by methyl groups on the aromatic ring of the salicylaldoxime ligand on the Mn-N-O-Mn torsion angle, as this parameter has been poorly studied [8,24,27]. So, we present in this work six new Mn(III) compounds based on the $\{Mn^{III}_3(\mu_3\text{-O})(R\text{-salox})_3\}^+$ fragment: $[Mn_3NaO(salox)_3(9\text{-AC})_2(EtOH)_3H_2O]_n\cdot 2EtOH$ (**1**), $[Mn_3NaO(3\text{-Me-salox})_3(9\text{-AC})_2(EtOH)_3H_2O]_n\cdot EtOH$ (**2**), $[Mn_6O_2(salox)_6(9\text{-AC})_2(EtOH)_2(H_2O)_2]\cdot 3EtOH$ (**3**), $[Mn_3O(3\text{-Me-salox})_3(9\text{-AC})(EtOH)_3(H_2O)]\cdot 1.8EtOH\cdot 3H_2O$ (**4**), $[Mn_6O_2(Me\text{-salox})_6(9\text{-AC})_2(EtOH)_4(H_2O)_2]\cdot 0.5H_2O$ (**5**), and $[Mn_6O_2(Et\text{-salox})_6(9\text{-AC})_2(EtOH)_4(H_2O)_2]\cdot 3EtOH$ (**6**). The compounds have been obtained from different H_2-R-salox ligands and the sodium or cesium salt of 9-anthracenecarboxylate that are shown in Scheme 2.



Scheme 2. Representation of the different organic ligands used in the synthesis of compounds **1**–**6**.

2. Results and Discussion

2.1. X-ray Crystal Structures

Crystallographic data for compounds **1**–**6** are summarized in the Supplementary Materials in Table S1. Oxidation number +3 has been determined for all manganese ions present in compounds **1**–**6** [31] through bond distances, charge balance, and bond valence sum (BVS) analysis. The results of this analysis are presented in Table S2.

2.1.1. $[Mn_3NaO(salox)_3(9\text{-}AC)_2(EtOH)_3H_2O]_n \cdot 2EtOH$ (**1**) and $[Mn_3NaO(3\text{-}Me\text{-}salox)_3(9\text{-}AC)_2(EtOH)_3H_2O]_n \cdot EtOH$ (**2**)

Compound **1** crystallizes in the C2/c group of the monoclinic system, while compound **2** crystallizes in the P-1 space group of the triclinic system. Figure 1 shows the crystalline structures of compounds **1** and **2**. They consist of chains of trinuclear units $\{Mn^{III}_3(\mu_3\text{-}O)(salox)_3\}^+$ connected by Na^+ ions along the [001] direction of the crystal lattice for **1** and [010] for **2**. In compound **1**, zigzag-type chains with inverted parallel planes alternate with contiguous intersecting planes at a dihedral angle of 57.3°, whereas in compound **2**, the chains consist of parallel inverted $\{Mn^{III}_3(\mu_3\text{-}O)(salox)_3\}^+$ planes. Both compounds have the same asymmetric unit $[Mn_3O(R\text{-}salox)_3(9\text{-}AC)_2(EtOH)_3H_2O]$, R = H for **1** and CH_3 for **2** (Figure 1a), with an architecture not previously observed. Given the structural similarity between **1** and **2**, only the structure of compound **1** is described as an example.

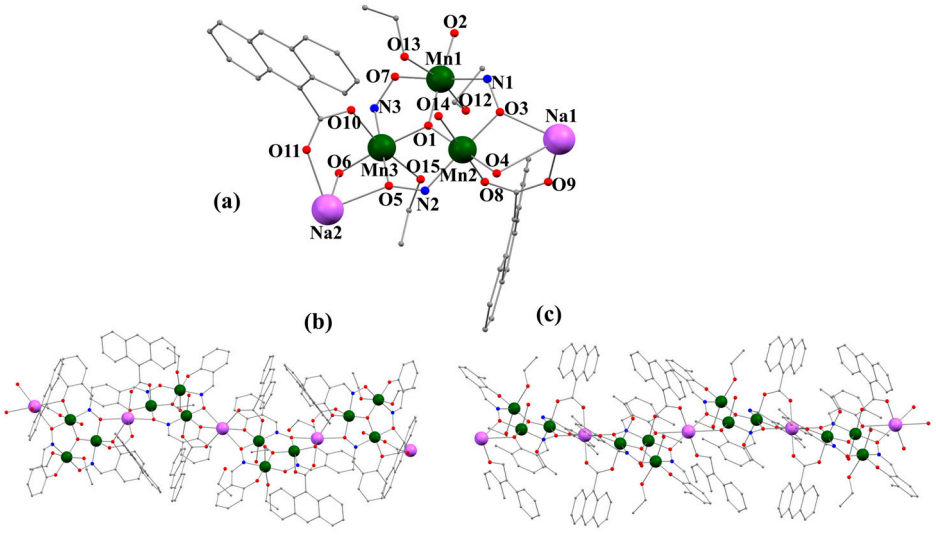


Figure 1. (**a**) Asymmetric units (partially labeled) for compounds **1** and **2**. (**b**,**c**) Chain structure representation of compounds **1** and **2**, respectively. Hydrogen atoms and solvent molecules have been omitted for clarity. Color code: dark green = Mn, pink = Na, red = O, blue = N, and gray = C.

The crystalline structure of **1** consists of chains of trinuclear units $\{Mn^{III}_3(\mu_3\text{-}O)(salox)_3\}^+$ connected through Na^+ ions. Table 1 lists the most important bond distances and angles for both compounds **1** and **2**. The Mn(III) ions form in **1** an almost equilateral triangle with distances between the vertices equal to 3.250 Å (Mn1···Mn2), 3.270 Å (Mn2···Mn3), and 3.232 Å (Mn1···Mn3), while in compound **2**, the observed distances are 3.262 Å (Mn1···Mn2), 3.279 Å (Mn2···Mn3), and 3.253 Å (Mn1···Mn3). Within each trinuclear unit, the three Mn(III) ions exhibit an octahedral geometry with Jahn–Teller distortions, with the equatorial planes of the octahedron lying within the same triangular plane. The four equatorial positions of the octahedron are occupied, in all three cases, by a bond with the μ_3-O^{2-} anion (O1), which also forms part of the plane formed by the three Mn(III) atoms with Mn-O1 distances ranging from 1.873(2) to 1.879 Å (1.8796(16) and 1.8916(18) Å for **2**), two bonds with nitrogen atoms (N1, N2, or N3) in the oxime group and oxygen atoms (O2, O4, or O6) in the phenoxo group of a $salox^{2-}$ ligand, and a bond with oxygen atoms (O3, O5, or O7) in the oxime group of another $salox^{2-}$ ligand. The Mn-N-O-Mn torsion angles are 28.6(3)° for Mn1-Mn2 (26.71(19)° for **2**), 5.4(3)° for Mn2-Mn3 (18.92(19)° for **2**), and 1.0(3)° for Mn1-Mn3 (21.6(2)° for **2**). The axial positions vary depending on the Mn(III) ion: for the Mn1 atom, these are occupied by two oxygen atoms, O12 and O13, from two ethanol molecules. On the other hand, the Mn2 and Mn3 ions each have an axial bond with the oxygen atoms O8 and O10, respectively, of two carboxylate ligands that act as bridges (in the *syn-syn* coordination mode) between these ions and the corresponding Na^+ cations (Na1 for Mn2 and Na2 for Mn3), forming the one-dimensional structure. The remaining axial positions are occupied by oxygen atom O14 of a water molecule in the case of the Mn2 ion and by oxygen atom O15 of an ethanol molecule in the case of Mn3.

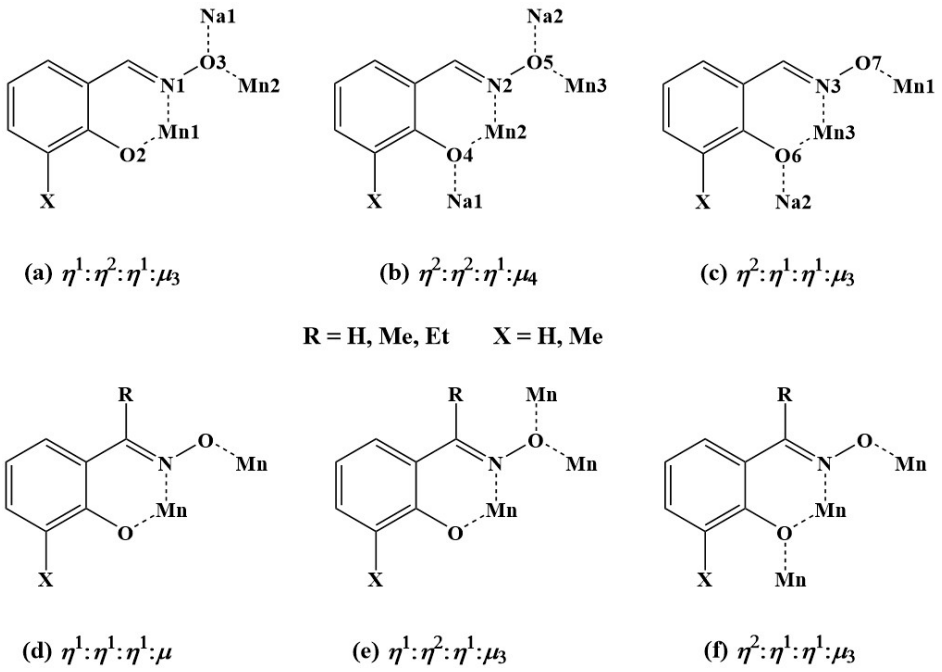
Table 1. Selected bond distances (Å) and angles (°) for compounds **1** and **2**.

	1	**2**		**1**	**2**
Mn1-O1	1.879(2)	1.8796(16)	Na1-O3	2.429(2)	2.3117(17)
Mn1-O2	1.863(2)	1.865(2)	Na1-O4	2.502(2)	2.8331(18)
Mn1-O7	1.903(2)	1.9043(19)	Na1-O9	2.332(2)	2.3321(17)
Mn1-O12	2.268(2)	2.3293(19)	Na1-O3″	2.429(2)	2.3117(17)
Mn1-O13	2.348(3)	2.3512(18)	Na1-O4″	2.502(2)	2.8331(18)
Mn1-N1	2.000(2)	2.002(2)	Na1-O9″	2.332(2)	2.3321(17)
Mn2-O1	1.879(2)	1.8831(16)	Na2-O5	2.454(2)	2.3548(19)
Mn2-O3	1.925(2)	1.9203(18)	Na2-O6	2.519(3)	2.7059(16)
Mn2-O4	1.883(2)	1.8794(17)	Na2-O11	2.353(3)	2.3335(16)
Mn2-O8	2.249(2)	2.2661(17)	Na2-O5′	2.454(2)	2.3548(19)
Mn2-O14	2.266(2)	2.2729(18)	Na2-O6′	2.519(3)	2.7059(16)
Mn2-N2	2.012(2)	2.003(2)	Na2-O11′	2.353(3)	2.3335(16)
Mn3-O1	1.873(2)	1.8916(18)	Mn1-O1-Mn3	118.95(11)	120.22(9)
Mn3-O5	1.912(2)	1.9188(16)	Mn1-O1-Mn2	119.77(11)	119.19(8)
Mn3-O6	1.873(2)	1.8838(19)	Mn2-O1-Mn3	121.25(11)	120.59(8)
Mn3-O10	2.158(2)	2.2053(17)	Mn2-O3-N1-Mn1	28.6(2)	26.71(19)
Mn3-O15	2.539(2)	2.3599(18)	Mn3-O5-N2-Mn2	5.4(3)	18.92(19)
Mn3-N3	2.010(2)	1.9979(19)	Mn1-O7-N3-Mn3	1.0(3)	21.6(2)

(′) = 1−x, y, 3/2−z (**1**); 1−x, −y, 1−z (**2**). (″) = 1−x, 1−y, 1−z (**1**); 1−x, 1−y, 1−z (**2**).

Each sodium cation, Na1 and Na2, exhibits an $[NaO_6]$ coordination environment constructed by O9 and O9′ (for Na1) or O11 and O11′ (for Na2) from two of the bridging carboxylate ligands, by O3 and O3′ (for Na1) or O5 and O5′ (for Na2) from the oxime groups of two different $salox^{2-}$ ligands, and by the phenoxo oxygen atoms O4 and O4′ (for Na1) or O6 and O6′ (for Na2) from two other $salox^{2-}$ ligands. The Na-O distances are in the range of 2.332(2)-2.502(2) Å for the Na1 atom (2.3117(17)-2.8331(18) Å in **2**) and in the range of 2.353(3)-2.519(3) Å for the Na2 atom (2.3335(16)-2.7059(16) Å in **2**). The three $salox^{2-}$ ligands in each trinuclear unit therefore exhibit three different coordination modes: one in the η^2:η^1:η^1:μ_3 mode (Scheme 3a), another in the η^2:η^2:η^1:μ_4 mode (Scheme 3b), and the remaining one in the η^1:η^2:η^1:μ_3 mode (Scheme 3c). The Na1 ion adopts a distorted

octahedral geometry (elongated axial position due to bonding with oxygen atoms O4 and O4′; Figure 2a), while the Na2 ion does not exhibit a regular geometry (Figure 2b). It is important to note that, in compound **2**, the Na2 ion exhibits an octahedral geometry, although it is axially distorted with the axial axis formed by O11 and O11′ (Figure 2c). The distortion of the coordination sphere of Na ions has been calculated using the SHAPE program based on continuous shape measures (CShMs) [32] yielding a deviation values of 3.95, 5.85, and 5.69 from the ideal octahedron (OC-6) for Na1 in **1**, Na2 in **1**, and Na2 in **2**, respectively (Table S4). This structural difference is due to the different dihedral angles between the contiguous $\{Mn^{III}_3(\mu_3\text{-}O)(salox)_3\}^+$ triangular planes in compounds **1** and **2**, as previously discussed.



Scheme 3. Coordination modes of the R-salox^{2-} ligands in compounds **1**–**6**.

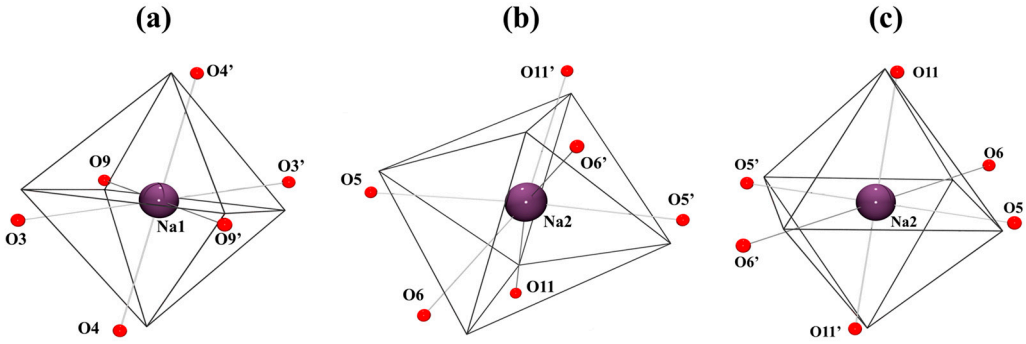


Figure 2. Coordination environments of cations (**a**) Na1, (**b**) Na2 for **1** and (**c**) Na2 for **2**.

2.1.2. Compound $[Mn_6O_2(salox)_6(9\text{-}AC)_2(EtOH)_2(H_2O)_2]\cdot 3EtOH$ (3·3EtOH)

The hexanuclear compound $[Mn_6O_2(salox)_6(9\text{-}AC)_2(EtOH)_2(H_2O)_2]\cdot 3EtOH$, shown in Figure 3, consists of two parallel trinuclear $\{Mn^{III}_3(\mu_3\text{-}O)(salox)_3\}^+$ planes, crystallographically related through an inversion center. The triangle formed by the three metal ions has sides with lengths of 3.267 Å (Mn1···Mn2), 3.245 Å (Mn2···Mn3), and 3.161 Å (Mn1···Mn3). The distances and angles of this compound are listed in Table 2

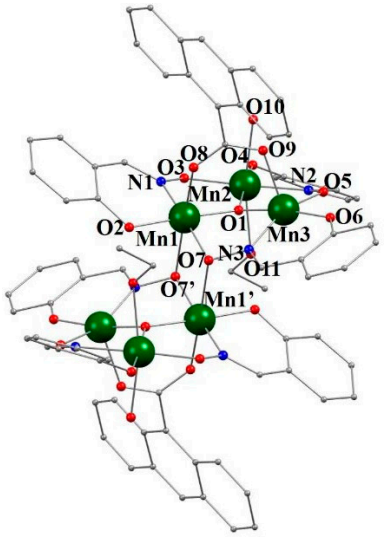


Figure 3. Structure of **3**, partially labeled. Hydrogen atoms have been omitted for clarity. Color code: dark green = Mn, red = O, blue = N, and gray = C.

Table 2. Most relevant bond distances (Å) and angles (°) of compounds **3**, **5**, and **6**.

	3	**5**	**6**
Mn1-O1	1.8781(18)	1.889(3)	1.876(3)
Mn1-O2	1.8825(19)	1.920(3)	1.904(3)
Mn1-O7	1.960(2)	1.955(3)	1.951(3)
Mn1-O8	2.161(2)	2.138(3)	2.171(3)
Mn1-N1	1.993(3)	2.007(5)	2.011(4)
Mn1-O7′)	2.332(2)	2.434(3)	2.415(3)
Mn2-O1	1.889(2)	1.880(3)	1.873(3)
Mn2-O3	1.931(2)	1.924(3)	1.921(3)
Mn2-O4	1.864(2)	1.877(4)	1.855(3)
Mn2-O10	2.272(2)	2.262(3)	2.373(5)
Mn2-O11	2.289(2)	2.246(3)	2.204(3)
Mn2-N2	2.023(2)	2.025(4)	2.001(4)
Mn3-O1	1.854(2)	1.890(3)	1.896(3)
Mn3-O5	1.927(2)	1.919(3)	1.916(3)
Mn3-O6	1.862(2)	1.868(4)	1.872(3)
Mn3-O9	2.132(2)	--	--
Mn3-O12	--	2.246(3)	2.231(3)
Mn3-O2′)	--	2.453(3)	2.395(3)
Mn1-O1-Mn2	120.27(11)	119.53(16)	120.07(14)
Mn1-O1-Mn3	115.79(11)	120.93(16)	120.54(14)
Mn2-O1-Mn3	120.21(9)	118.42(13)	118.40(13)
Mn1-O2-Mn3′)	--	118.27(12)	118.75(12)
Mn1-O7-Mn1′)	98.05(8)	94.23(12)	96.48(11)
Mn2-O3-N1-Mn1	27.7(2)	28.9(4)	30.3(3)
Mn3-O5-N2-Mn2	21.8(3)	34.7(4)	37.3(3)
Mn1-O7-N3-Mn3	24.7(2)	41.9(3)	47.3(3)

(′) = 1−x, 1−y, 1−z (**3**); 1−x, 1−y, −z (**5**); 1−x, 1−y, 1−z (**6**).

The two identical planes are connected via the two bonds between Mn1 and Mn1′ atoms with the bridging oxygen atoms O7′ and O7, respectively, from the oxime group of the corresponding salox^{2-} ligand of the opposite triangular plane, which exhibit a η^1:η^2:η^1:μ_3 coordination mode (Scheme 3e).

Within each triangular unit $\{Mn^{III}_3(\mu_3\text{-}O)(salox)_3\}^+$, the μ_3-O^{2-} (O1) anion, which is located at 0.210 Å above the plane formed by the three metal atoms, coordinates with the three Mn(III) ions. The three salox^{2-} ligands act as bridges between two neighboring

coplanar Mn(III) ions through the nitrogen (N1, N2, and N3) and oxygen (O3, O5, and O7) atoms of the oxime group, and also interact via the oxygen of the phenoxo group (O2, O4, and O6), exhibiting η^1:η^1:η^1:μ or η^1:η^2:η^1:μ_3 coordination modes as shown in Scheme 3d,e, respectively. The torsion of the Mn–N–O–Mn angles is, in all cases, less than 31° (Mn1-Mn2 = 27.7(2)°, Mn2-Mn3 = 21.8(3)°, and Mn1-Mn3 = 24.7(2)°). Therefore, the Mn-Mn magnetic exchange via the salox^{2-} ligands is expected to be antiferromagnetic. The Mn1 and Mn2 atoms have an octahedral coordination environment with Jahn–Teller distortions, while the Mn3 atom has a pyramidal geometry. The equatorial planes of the geometry of the three ions coincide with the triangular plane $\{Mn^{III}_3(\mu_3\text{-O})(salox)_3\}^+$. For Mn2, the axial positions are occupied by an oxygen atom from a water molecule (O10) and an oxygen atom from an EtOH molecule (O11). For Mn1, one of the axial positions is occupied, as mentioned before, by the oximate oxygen atom O7′ connecting the two trinuclear planes. The remaining axial position is occupied by one of the oxygen atoms (O8) from a 9-AC anion, which also binds, through a *syn-syn* coordination, to the Mn3 ion via O9 occupying the corresponding axial position. The axial axes of all manganese atoms are almost parallel to each other and perpendicular to the $\{Mn^{III}_3(\mu_3\text{-O})(salox)_3\}^+$ planes.

The H_2O and EtOH molecules coordinated to Mn2 form intramolecular hydrogen bridges. The hydrogen atoms H11A of the coordinated EtOH molecules form a bond with the nearest phenolic oxygen atom O2, belonging to one of the salox^{2-} ligands of a neighboring triangle. In the case of the H_2O molecules, each hydrogen H10A forms a bridge with the oxygen atom O9 of the neighboring carboxylate, while the H10B atoms interact with the oxygen atom O1M of a free EtOH molecule. The hydrogen of this solvent molecule also interacts via a hydrogen bridge with the oximate oxygen atom O5 of a salox^{2-} ligand belonging to a neighboring hexanuclear unit, forming chains of $[Mn_6O_2(salox)_6(9\text{-AC})_2(EtOH)_2(H_2O)_2]$ molecules along the [010] direction of the cell (Figure S1). The structural parameters of these supramolecular contacts are listed in Table S3.

2.1.3. Compound $[Mn_3O(3\text{-Me-salox})_3(9\text{-AC})(EtOH)_3(H_2O)]\cdot 1.8EtOH\cdot 3H_2O$ (**4**·1.8EtOH·3H_2O)

The asymmetric unit of coordination compound **4**, which crystallizes in the P-1 space group of the triclinic system, consists of two molecules $[Mn_3O(3\text{-Me-salox})_3(9\text{-AC})(EtOH)_3(H_2O)]$, referred to as A and B. These molecules exhibit differences in structural parameters but identical coordination. The most relevant distances and angles of molecules A and B in compound **4** are listed in Table 3. Figure 4 shows the A molecule.

Table 3. Selected bonds distances (Å) and angles (°) in fragments A and B of **4**.

Compound 4					
	A	**B**		**A**	**B**
Mn1-O1	1.886(2)	1.864(2)	Mn3-O1	1.867(2)	1.890(2)
Mn1-O2	1.857(2)	1.864(2)	Mn3-O5	1.921(2)	1.897(2)
Mn1-O7	1.940(2)	1.912(3)	Mn3-O6	1.853(3)	1.889(2)
Mn1-O8	2.240(2)	2.095(2)	Mn3-O9	2.220(2)	2.224(2)
Mn1-O10	2.270(3)	3.769(3)	Mn3-O13	2.349(3)	2.282(3)
Mn1-N1	1.998(3)	2.005(3)	Mn3-N3	2.012(3)	2.008(3)
Mn2-O1	1.869(2)	1.887(2)	Mn1-O1-Mn2	121.09(12)	120.64(11)
Mn2-O3	1.916(2)	1.928(2)	Mn1-O1-Mn3	116.73(12)	114.59(11)
Mn2-O4	1.866(2)	1.874(2)	Mn2-O1-Mn3	120.28(12)	119.46(12)
Mn2-O11	2.283(3)	2.231(3)	Mn2-O3-N1-Mn1	28.9(3)	15.6(3)
Mn2-O12	2.353(3)	2.233(3)	Mn3-O5-N2-Mn2	26.7(3)	16.4(3)
Mn2-N2	2.021(3)	2.006(3)	Mn1-O7-N3-Mn3	32.1(3)	18.9(3)

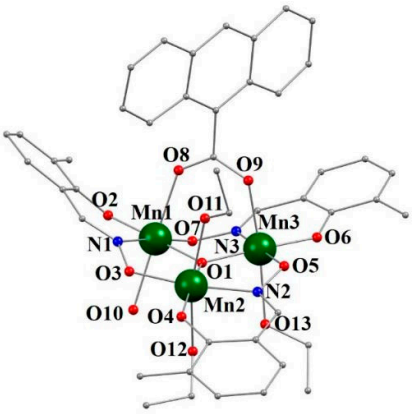


Figure 4. Partially labeled illustration of the molecule $[Mn_3O(3\text{-Me-salox})_3(9\text{-AC})(EtOH)_3(H_2O)]$(A) in compound **4**. Hydrogen atoms have been omitted for clarity.

Each $[Mn_3O(3\text{-Me-salox})_3(9\text{-AC})(EtOH)_3(H_2O)]$ A or B molecule shows the $\{Mn^{III}{}_3(\mu_3\text{-}O)(3\text{-Me-salox})_3\}^+$ plane coplanar with the equatorial bases of the axially distorted octahedral geometry of the three Mn(III) ions. The Mn1 and Mn3 ions are connected by a bridging 9-AC ligand in a *syn-syn* coordination mode by the oxygen atoms O8 and O9, which occupy one of the axial positions of each of the two Mn(III) ions. The remaining axial positions are occupied by O10 from a water molecule in the case of Mn1, and by O13 from an EtOH molecule in the case of the Mn3 ion. The Jahn–Teller axis of the Mn2 atom is established by the oxygen atoms O11 and O2 of two EtOH molecules.

The distances in the triangle between the three Mn(III) ions are 3.269 Å, 3.240 Å, and 3.196 Å in fragment A and 3.259 Å, 3.262 Å, and 3.159 Å in fragment B. The torsion angles of molecules A and B differ significantly. The Mn-N-O-Mn torsions are 28.9(3)°, 26.7(3)°, and 32.1(3)° in molecule A, and 15.6°, 16.4(3)°, and 18.9° in molecule B. Therefore, the $\{Mn^{III}{}_3(\mu_3\text{-}O)(3\text{-Me-salox})_3\}^+$ plane in molecule B is much less distorted than in molecule A. This causes the axial bonds Mn1B-O8B and Mn1B-10B to be much shorter and considerably longer, respectively, compared to the equivalent ones in molecule A.

The solvent molecules coordinated to the Mn(III) ions form hydrogen bonds. The structural parameters are collected in Table S3 (Supplementary Materials). For fragment A, the oxygen atom O10A of the water molecule forms a bond with one of the water molecules (O1W) that co-crystallizes with the compound and another bond with the oxygen atom O6B of the phenolate group of one of the 3-Me-salox^{2-} ligands from the other neutral trinuclear fragment. The hydrogen atoms bonded to the oxygen atoms O11A, O12A, and O13A of the three coordinated ethanol molecules interact with oxygen atoms O9A, O10A, and O1W, which are from the bridging carboxylate ligand, the water molecule bonded to the Mn1 ion and the free water molecule, respectively. In fragment B, the water coordinated to the Mn1 ion (O10B) forms bridges with the oxygen atoms O5A and O9A of the other trinuclear fragment. One of the two ethanol atoms (O12B) coordinated to the Mn2 atom forms a hydrogen bond with the water molecule (O10B). The other solvent molecule interacts via O11B with the water molecule of crystallization O1W. The hydrogen bonded to the oxygen atom O13B of EtOH coordinated to the Mn3 atom also forms a bridge with the water molecule O10B. As a result of these supramolecular interactions, chains of $[Mn_3O(3\text{-Me-salox})_3(9\text{-AC})(EtOH)_3(H_2O)]$ units are constructed along the [100] direction of the crystal lattice (Figure S2).

2.1.4. Compounds $[Mn_6O_2(Me\text{-salox})_6(9\text{-AC})_2(EtOH)_4(H_2O)_2]\cdot 0.5H_2O$ (**5**·0.5H_2O) and $[Mn_6O_2(Et\text{-salox})_6(9\text{-AC})_2(EtOH)_4(H_2O)_2]\cdot 3EtOH$ (**6**·3EtOH)

Figure 5 shows the structure of compounds **5** and **6**. As previously explained, these two compounds are obtained starting from either the Na^+ carboxylate or Cs^+ carboxylate salts. Although the hexanuclear core of compound **6**·3EtOH, has been published previously [33], there are differences with respect to the crystallization solvent molecules in

the unit cell; for compound **6**·3EtOH, three molecules of EtOH crystallize, whereas in the previously published results, compounds with the same hexanuclear core crystallize 0.66 molecules of EtOH and 0.33 molecules of H_2O.

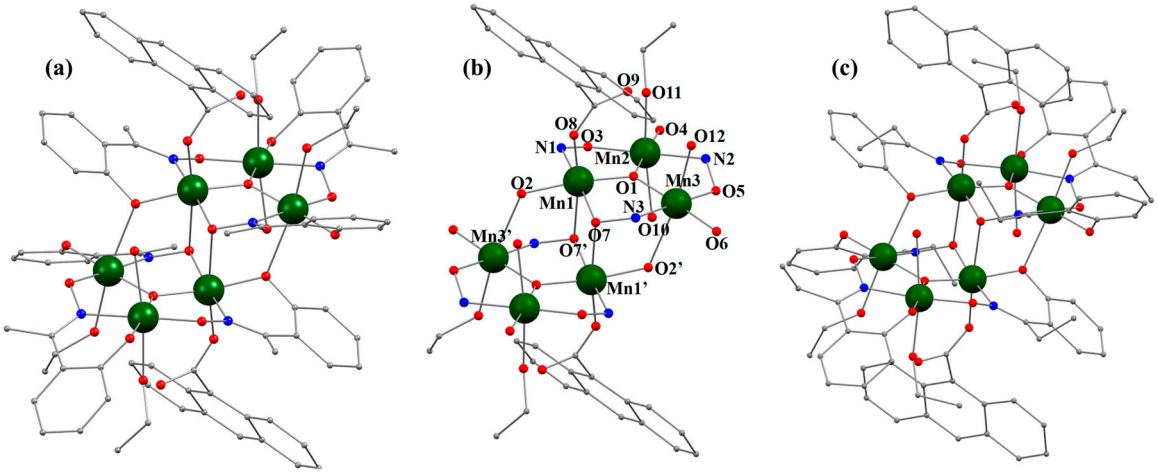


Figure 5. (**a**,**c**) Hexanuclear compounds **5** and **6**, respectively. Figure (**b**) represents the partially labeled hexanuclear core of these two structures. The hydrogen atoms and solvent molecules have been omitted for clarity. Color code: dark green = Mn, red = O, blue = N, and gray = C.

Given the high similarity between the structures of compounds **5** and **6**, the structural description of the hexanuclear cores are provided using compound **5** as the example.

The structure of the compound $[Mn_6O_2(Me\text{-}salox)_6(9\text{-}AC)_2(EtOH)_4(H_2O)_2]$ (**5**) consists of two identical parallel planes $\{Mn^{III}{}_3(\mu_3\text{-}O)(Me\text{-}salox)_3\}^+$ related by an inversion center. BVS calculations and the charge balance of the compound indicate that the six metals are in the +3-oxidation state (Table S2). Additionally, all Mn(III) ions exhibit an octahedral coordination geometry with axial Jahn–Teller distortions. The axial axes are almost completely parallel to each other and perpendicular to the two $\{Mn^{III}{}_3(\mu_3\text{-}O)(Me\text{-}salox)_3\}^+$ planes. In the $[Mn]_3$ triangles, the distances between the Mn(III) atoms are similar, being 3.256 Å (Mn1···Mn2), 3.238 Å (Mn2···Mn3), and 3.287 Å (Mn1···Mn3) for compound **5**, and 3.248 Å (Mn1···Mn2), 3.237 Å (Mn2···Mn3), and 3.275 Å (Mn1···Mn3) for compound **6**.

In each $\{Mn^{III}{}_3(\mu_3\text{-}O)(Me\text{-}salox)_3\}^+$ unit, the plane formed by the $[Mn_3]$ ions coincides with the equatorial plane of the coordination environment of these ions. One of the four equatorial positions in the coordination sphere of the Mn(III) ions is occupied by the $\mu_3\text{-}O^{2-}$ anion (O1), which is found slightly above the plane formed by the three metal atoms (0.116 Å for **5** and 0.109 Å for **6**). The remaining three equatorial positions are occupied by a phenoxo oxygen atom (O2, O4, or O6), a nitrogen atom (N1, N2, or N3) from the Me-salox^{2-} ligand, and an oxygen atom from the oximate group (O3, O5, or O7) of another Me-salox^{2-} ligand. The oximate group of each Me-salox^{2-} ligand acts as a bridge between two coplanar Mn(III) ions, with Mn-N-O-Mn torsion angles of 28.9(4)° for Mn1-Mn2 (30.3(3)° for **6**), 34.7(4)° for Mn2-Mn3 (37.3(3)° for **6**), and 41.9(3)° for Mn1-Mn3 (47.3(3)° for **6**). The axial positions of the Mn1 ions are formed by O8 from a terminal anthracenecarboxylate and O7′ from the oximato group of an Me-salox^{2-} anion placed at the opposite plane. For the Mn2 atom, the axial positions are occupied by two oxygen atoms, O10 and O11, which are part of a water molecule and an EtOH molecule, respectively. The axial bond of Mn3 with oxygen atom O2′ of the phenoxo group from one of the Me-salox^{2-} entities also serves as a connection between the two $\{Mn^{III}{}_3(\mu_3\text{-}O)(Me\text{-}salox)_3\}^+$ planes. The remaining axial position is occupied by oxygen atom O12 from an EtOH molecule. Therefore, two of the six Me-salox^{2-} ligands exhibit a $\eta^1{:}\eta^1{:}\eta^1{:}\mu$ coordination (Scheme 3d), acting as bridges between pairs of Mn(III) ions within the same triangular unit, and the remaining four also connect the two trinuclear planes via oximato group oxygens in the $\eta^1{:}\eta^2{:}\eta1{:}\mu_3$ coordination mode (Scheme 3e) or the hydroxo group ($\eta^2{:}\eta^1{:}\eta^1{:}\mu_3$ coordination mode; Scheme 3f).

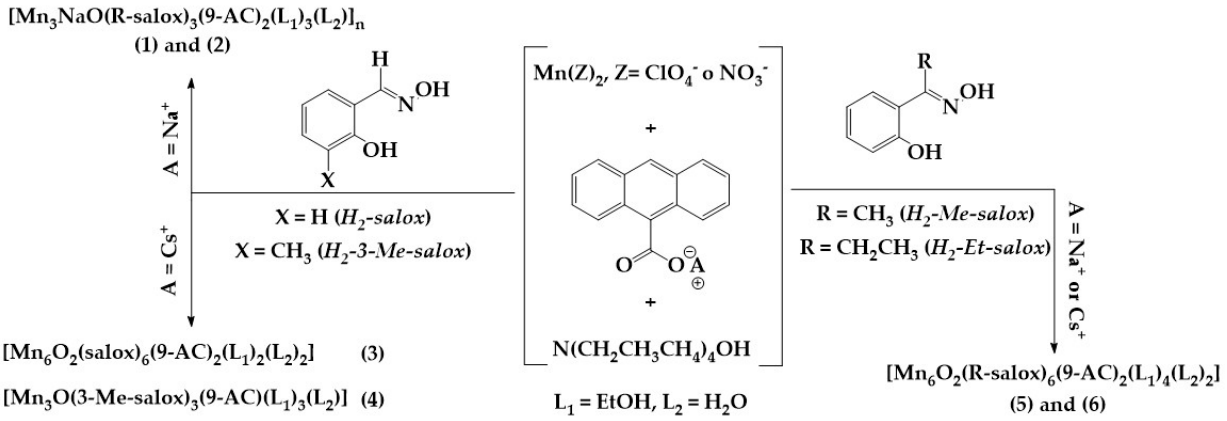
In compound **5**, different intramolecular hydrogen bonds are observed. On the one hand, oxygen atom O9 of the carboxylate interacts with hydrogen atoms H11A and H12A of the two EtOH molecules coordinated to Mn2 and Mn3, respectively. On the other hand, the water coordinated to the Mn2 ion forms a hydrogen bond through hydrogen atom H10A with oxygen atom O2′ and through the H10B atom with the oxygen atom of a free water molecule (O1W). In the case of compound **6**, the H10B atom interacts with oxygen atom O7 of the oximate group of a nearby Me-salox^{2-} ligand, while the hydrogen atom H10A forms a bond with a free EtOH molecule (O1M). Although it has not been possible to assign the hydrogen atoms of the free EtOH molecule (O1M), it is observed that this molecule forms a hydrogen bond with another EtOH molecule (O1M′), leading to a 1D arrangement of $[Mn_6O_2(Et\text{-}salox)_6(9\text{-}AC)_2(EtOH)_4(H_2O)_2]$ units along the [110] direction of the crystalline network. The distances and angles of these contacts are listed in Table S3.

It should be highlighted that the differences in the number and type of crystallization solvent molecules between compound **6**·3EtOH and the previously published compound **6**·0.66EtOH·0.33H_2O [33] have been observed, and this affects the structure of the hexanuclear complex and, possibly, its magnetic properties. In the case of complex **6**·3EtOH, the Mn-N-O-Mn torsion angles within the $[Mn^{III}]_3$ plane are 30.3° (Mn1-Mn2), 37.3° (Mn2-Mn3), and 47.9° (Mn1-Mn3), whereas for the previously published compound **6**·0.66EtOH·0.33H_2O, the torsion angles are 42.30° (Mn1-Mn2), 25.6° (Mn2-Mn3), and 39.3° (Mn1-Mn3).

2.1.5. Structural Discussion

In compounds **1**–**6**, BVS calculations determined an oxidation state of +3 for the manganese ions present, even though Mn(II) was used initially. The oxidation of the Mn(II) cation is due to atmospheric oxygen. The deprotonation of the R-salicyladoxime species occurs via the anions of the starting Mn(II) salts and the bases present in the reaction medium. All attempts to obtain the manganese (II) anthracenecarboxylate salt failed. Therefore, it was decided to start with Mn(II) salts with nitrate and perchlorate anions, which are less susceptible to coordinate with this metal [34].

As previously mentioned, to obtain new topologies of compounds based on the triangular unit $\{Mn^{III}_3(\mu_3\text{-}O)(R\text{-}salox)_3\}^+$, new variables were introduced into the synthesis process. On one hand, the H_2-3-Me-salox ligand, with a CH_3 group at position 3 of the phenyl ring and the oxime group at position 1, was used. Another variable introduced was the alkali cation used in the starting salt of the anthracenecarboxylate anion. As summarized in Scheme 4, for the R-salox^{2-} ligands with X = H and 3-Me, both having a hydrogen bonded to the carbon of the oxime group, it was observed that using sodium salt yielded chain-like structures $[Mn_3NaO(salox)_3(9\text{-}AC)_2(EtOH)_3H_2O]_n$·2nEtOH (**1**·2EtOH) and $[Mn_3NaO(3\text{-}Me\text{-}salox)_3(9\text{-}AC)_2(EtOH)_3H_2O]_n$·nEtOH (**2**·EtOH) consisting of triangles connected by Na^+ cations. On the other hand, the use of the cesium carboxylate salt did not produce chain-like compounds; instead, the hexanuclear compound $[Mn_6O_2(salox)_6(9\text{-}AC)_2(EtOH)_2\ (H_2O)_2]$·3EtOH (**3**·3EtOH) and the trinuclear compound $[Mn_3O(3\text{-}Me\text{-}salox)_3(9\text{-}AC)(EtOH)_3(H_2O)]$·1.8EtOH·3$H_2O$ (**4**·1.8EtOH·3H_2O) were obtained, due to the larger ionic radius of the Cs^+ cation compared to Na^+. For the Me-salox^{2-} and Et-salox^{2-} ligands, the hexanuclear compounds $[Mn_6O_2(Me\text{-}salox)_6(9\text{-}AC)_2(EtOH)_4(H_2O)_2]$·0.5$H_2O$ (**6**·0.5H_2O) and $[Mn_6O_2(Et\text{-}salox)_6(9\text{-}AC)_2(EtOH)_4(H_2O)_2]$·3EtOH (**6**·3EtOH), respectively, were obtained regardless of whether the cesium or sodium anthracenecarboxylate salt was used. This is due to the distortion caused by the alkyl substituent groups on the oxime group of the different R-salox^{2-} ligands on the Mn-N-O-Mn torsion angles.



Scheme 4. Synthetic routes to obtain compounds **1**–**6**.

Generally, hexanuclear compounds with two $\{Mn^{III}_3(\mu_3\text{-}O)(R\text{-}salox)_3\}^+$ units present two types of structures. For small substituent group volumes (R = H), as in compound **3**, the two triangles tend to connect through two oxime bridges, with each Mn(III) ion exhibiting a square pyramidal coordination, while the other two Mn(III) ions have a distorted octahedral geometry [7,35]. The coordination of the carboxylate ligand in this type of architecture is syn-syn. On the other hand, when using R-salox^{2-} with more voluminous groups, as in compounds **5** (R = Me) and **6** (R = Et), the inter-triangular Mn–O bridge distances with the oxime group oxygen atom tend to decrease due to the increased Mn–N–O–Mn distortion, and the connection between triangles also occurs via two phenolate bridges. As a result, all three Mn(III) ions are in a distorted octahedral environment. Another structural consequence of varying the R-salox^{2-} ligand is that, as the volume of the R group increases, the triangles lose planarity, the carboxylate cannot coordinate in a syn-syn mode, and instead adopts a terminal mode, with the axial position of the Mn(III) occupied by a solvent molecule [6]. However, the different coordination modes of the carboxylate anion do not significantly influence the magnetic properties of the compounds.

2.2. Magnetic Properties

2.2.1. *dc* Magnetic Studies

The measurements of the magnetic susceptibility of compounds **1**–**6** were carried out in a range of temperatures, (2–300) K, under a magnetic field (dc) of 0.5 T for compound **1** and 0.3 T for compounds **2**–**6**. Figure 6a shows the thermal dependence of the susceptibility of these compounds in the form of the $\chi_M T$ product.

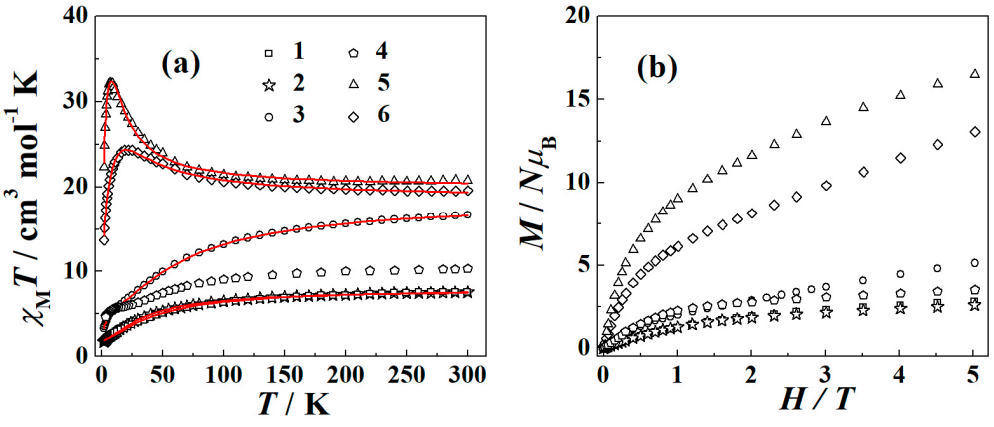
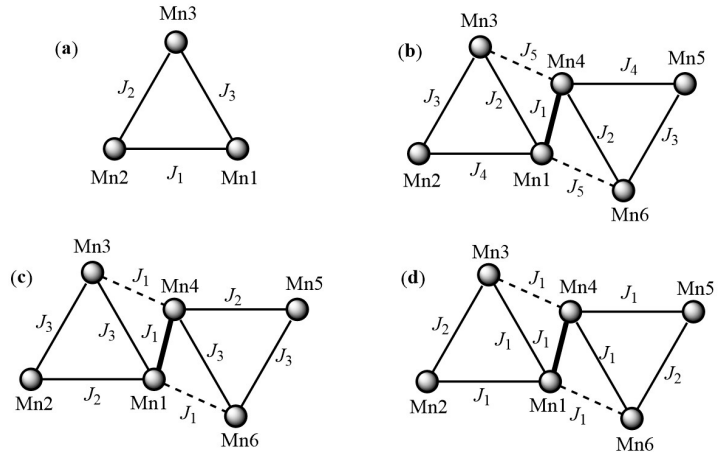


Figure 6. (**a**) $\chi_M T$ curves as a function of T for compounds **1**–**6**. The solid lines represent the theoretical fits according to the models discussed in the text. (**b**) Curves of magnetization ($M/N\mu_B$) as a function of the external magnetic field (H) for compounds **1**–**6**. The symbols have the same meanings as in (**a**).

Compounds **1** and **2** exhibit a $\chi_M T$ value at room temperatures of 7.51 and 7.49 $cm^3\ mol^{-1}$ K, respectively, which is significantly lower than the expected value for three non-interacting high-spin Mn(III) centers (9 $cm^3\ mol^{-1}$ K for S = 2 and g = 2.0). In both complexes, the $\chi_M T$ curve remains constant as the temperature decreases to approximately 90 K. From this temperature, a more pronounced drop in the curves is observed, reaching a $\chi_M T$ value of 1.60 $cm^3\ mol^{-1}$ K for **1** and 1.87 $cm^3\ mol^{-1}$K for **2** at 2 K. The experimental data could be fitted using a model assuming three types of magnetic interactions (J_1, J_2, and J_3, Equation (1), Scheme 5a) between each pair of neighboring Mn(III) ions within each triangle, through the oxo group (O1) and the corresponding oxime groups of the ligands derived from salicylaldoxime.

$$H = -J_1(S_1 \cdot S_2) - J_2(S_2 \cdot S_3) - J_3(S_1 \cdot S_3) \quad (1)$$



Scheme 5. Representation of the magnetic interaction models based on the Hamiltonians described in the text used to fit the experimental data of $\chi_M T$ as a function of T (**a**) for compounds **1** and **2**, (**b**) for **3**, (**c**) for **5** and **6**, and (**d**) for **6**·0.66EtOH·0.33H_2O (**d**) [33].

The obtained values from the fittings indicate a set of antiferromagnetic interactions promoted by the torsion angles less than 30.4° within the triangles, being $J_1 = -7.3\ cm^{-1}$, mboxemphJ$_2 \approx J_3 = -2.5\ cm^{-1}$, g = 1.90 with an error R = 5.2 × 10^{-4}, and S = 1 with an excited state S = 2 at 0.32 cm^{-1} for **1**. For compound **2**, the values are $J_1 = -6.02\ cm^{-1}$, $J_2 \approx J_3 = -2.2\ cm^{-1}$, g = 1.88 with R = 2.1 × 10^{-4}, and S = 1, with a very close energy excited state, S = 2 (at 0.43 cm^{-1}).

The susceptibility vs. temperature plot of hexanuclear compound **3** shows a $\chi_M T$ value of 16.62 $cm^3\ mol^{-1}$ K at 300 K, slightly lower than the expected 18 $cm^3\ mol^{-1}$ K for six fully uncoupled Mn(III) ions at this temperature, indicating possible antiferromagnetic interactions. As the temperature decreases, the $\chi_M T$ curve gradually decreases as well. At approximately 10 K, a change in the slope of the curve is observed, and for temperatures below this, $\chi_M T$ drops more abruptly, reaching a $\chi_M T$ value of 3.29 $cm^3\ mol^{-1}$ K at 2 K. The experimental measurements could be fitted based on a model that assumes five different types of magnetic interactions, depending on the different bridges between Mn(III) ions, as described in Equation (2) and Scheme 5b.

$$H = -J_1(S_1 \cdot S_4) - J_2(S_1 \cdot S_3 + S_4 \cdot S_6) - J_3(S_2 \cdot S_3 + S_5 \cdot S_6) - J_4(S_1 \cdot S_2 + S_4 \cdot S_5) - J_5(S_3 \cdot S_4 + S_1 \cdot S_6) \quad (2)$$

The best fitting parameters obtained yield values of $J_1 = +3.8\ cm^{-1}$, $J_2 = -6.0\ cm^{-1}$, $J_3 = -9.9\ cm^{-1}$, $J_4 = -5.2\ cm^{-1}$, $J_5 = +1.2\ cm^{-1}$, g = 2.04 with R = 7.3 × 10^{-6}, and S = 2 (with an excited state S = 3 located at 4.29 cm^{-1}). Therefore, the intra-triangular magnetic exchanges (with observed torsion angles less than 30.4°) are of the antiferromagnetic type, while the magnetic interaction between triangles is of the ferromagnetic type.

The $\chi_M T$ versus temperature curve of compound **4**, for only one of the triangular units, shows a value of 10.30 cm^3 mol^{-1} K at T = 300 K, slightly above the expected value for three fully uncoupled Mn(III) ions. As the temperature decreases, the curve declines, suggesting the presence of antiferromagnetic intramolecular couplings. $\chi_M T$ reaches a value of 3.73 cm^3 mol^{-1} K at T = 2 K. Due to the fact that **4** is composed by two [Mn_3O(3-Me-salox)$_3$(9-AC)(EtOH)3(H_2O)] molecules with different structural parameters, an analysis of the susceptibility data has not been possible as it requires extensive parameterization.

For compounds **5** and **6**, the $\chi_M T$ values at room temperature are 20.75 and 19.55 cm^3 mol^{-1} K, respectively, above the expected value at this temperature (18 cm^3 mol^{-1} K), suggesting the existence of ferromagnetic coupling. As the temperature decreases, the curves gradually increase to 21.39 cm^3 mol^{-1} K for **5** and 20.80 cm^3 mol^{-1} K for **6** at T = 100 K. From this temperature, the $\chi_M T$ values rise rapidly, reaching maximum values of 32.16 cm^3 mol^{-1} K at T = 7 K (**5**) and 24.37 cm^3 mol^{-1} K at T = 19 K (**6**). Subsequently, the curves drop to $\chi_M T$ values of 22.30 and 13.67 cm^3 mol^{-1} K for **5** and **6**, respectively, at T = 2 K. The fitting of the experimental susceptibility measurements was performed for both compounds using Equation 3, considering three different types of magnetic exchange interactions (J), as represented in Scheme 5c. J_1 corresponds to the coupling between the two [Mn_3] triangles, J_2 to the coupling between Mn1 and Mn2 ions mediated by the oxime groups and the oxo bridge with torsion angles of 28.9° (**5**) and 30.3° (**6**), which is below the magic angle region, and J_3 corresponds to the intra-triangular coupling between Mn1-Mn3 and Mn2-Mn3 ions, with torsion angles within the ferromagnetic range for both compounds.

$$H = -J_1(S_1 \cdot S_4 + S_3 \cdot S_4 + S_1 \cdot S_6) - J_2(S_1 \cdot S_2 + S_4 \cdot S_5) \\ -J_3(S_1 \cdot S_3 + S_2 \cdot S_3 + S_4 \cdot S_6 + S_5 \cdot S_6) \quad (3)$$

The fittings performed indicate values of J_1 = +2.3 cm^{-1}, J_2 = −2.0 cm^{-1}, J_3 = +1.7 cm^{-1}, and g = 2.09 with R = 1.2 × 10^{-4} and S = 5 with very close excited states, S = 6 (at 0.24 cm^{-1}) and S = 4 (at 0.49 cm^{-1}), for complex **5**. For compound **6**, the values obtained are J_1 = +3.18 cm^{-1}, J_2 = −5.2 cm^{-1}, J_3 = +3.5 cm^{-1}, g = 2.03 with R = 5.8 × 10^{-5}, and S = 4 with an excited state of S = 5 at 0.22 cm^{-1}.

The results for compound **6**·3EtOH can be compared with those reported for **6**·0.66EtOH·0.33H_2O, where $\chi_M T$ versus temperature curves show similar $\chi_M T$ values at T = 300 K, being 19.55 cm^3 mol^{-1} K for **6**·3EtOH and 19.80 cm^3 mol^{-1} K for **6**·0.66EtOH·0.33H_2O. As the temperature decreases, the $\chi_M T$ curves of both compounds increase, but while the maximum $\chi_M T$ value for complex **6**·3EtOH is 24.37 cm^3 mol^{-1} K (at T = 100 K), compound **6**·0.66EtOH·0.33H_2O shows a maximum $\chi_M T$ value of 50.53 cm^3 mol^{-1} K (at T ≈ 10 K). The fitting of the experimental $\chi_M T$ data of compound **6**·0.66EtOH·0.33H_2O was performed considering a Hamiltonian with only two magnetic coupling constants (Scheme 5d), yielding parameters of J_1 = +3.50 cm^{-1} and J_2 = −1.80 cm^{-1}, g = 2.00, and showing a ground state of S = 12 with an excited state of S = 11 at 0.79 cm^{-1}. Comparing these results with those obtained for compound **6**·3EtOH (J_1 = +3.18 cm^{-1}, J_2 = −5.2 cm^{-1}, J_3 = +3.5 cm^{-1}, g = 2.03, and S = 4) clearly shows that structural variations promote magnetic coupling between the Mn(III) ions with a greater contribution of antiferromagnetic exchanges in **6**·3EtOH, resulting in a lower-magnitude ground state, Table 4.

Magnetization measurements for compounds **1**–**6** were performed under magnetic fields in the range of [0–5] T at a temperature of 2 K. As shown in Figure 6b, no magnetic saturation was observed in any case, confirming the presence of spin-excited states very close in energy to the ground state. This is the reason why the experimental data could not be fitted.

Table 4. Torsion angles (°), expected and observed net coupling, and J_i interactions.

Compound	Mn-O-N-Mn (°) [a]	Expected Net Coupling	Observed Net Coupling	*Ji* (*i* = 1–5) (cm^{-1}) [c]
1	28.6, 5.4, 1.0	AF	AF	−7.3, −2.5, −2.5
2	26.7, 18.9, 21.6	AF	AF	−6.02, −2.2, −2.2
3	27.7, 21.8, 24.7	AF	AF	+3.8, −6.0, −9.9, −5.2, +1.2
4-A [b]	28.9, 26.7, 32.1	AF	-	-
4-B [b]	15.6, 16.4, 18.9	AF	-	-
5	28.9, 34.7, 41.9	AF/F	F	+2.3, −2.0, +1.7
6·3EtOH	30.3, 37.3, 47.3	AF/F	F	+3.18, −5.2, +3.5
6·0.66EtOH·0.33H_2O [d]	42.3, 25.6, 39.3	AF/F	F	+3.5, −1.8

[a] Torsion angle within each triangular unit. [b] Compound **4** is formed by two [Mn_3O(3-Me-salox)$_3$(9-AC)(EtOH)3(H_2O)] molecules with different structural parameters. The analysis of the susceptibility data has not been possible as it requires extensive parameterization. [c] The magnetic interaction, *Ji*, did not correspond to the same set in all the compounds; see the magnetic interaction representation in Scheme 5. [d] Compound reported in the reference [33].

2.2.2. Dynamic Magnetic Measurements (*ac*)

For compounds **5** and **6**, *ac* magnetization was performed at frequencies in the range of (5–1488) Hz for **5** and (1–1488) Hz for **6**, applying an *ac* field of 4×10^{-4} T. Figure 7 shows the thermal dependencies of the in-phase (χ_M') and out-of-phase (χ_M'') components of susceptibility for both compounds. Maxima were observed at approximately 3 K for **5** and 3.4 K for **6**. In the graphs of the two susceptibility components of compound **5**, a shoulder at higher temperatures can be discerned, as observed in other similar Mn(III) compounds [36], which may indicate the presence of a second relaxation process. However, the analysis of the dynamic magnetic properties of compound **5** was performed, only considering the maxima observed at low temperatures.

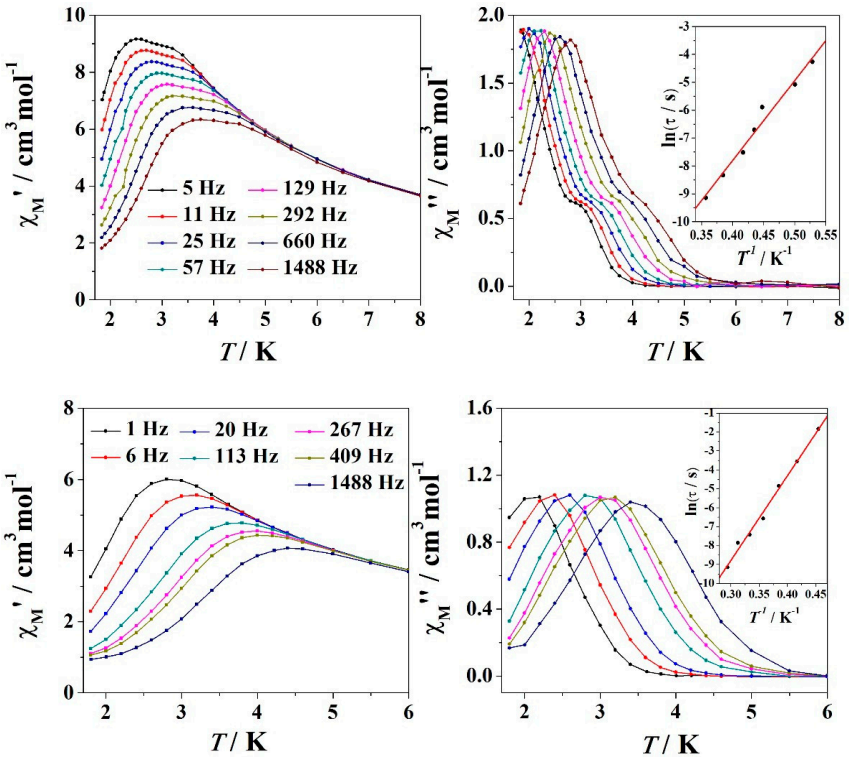


Figure 7. Curves χ_M' (**left**) and χ_M'' (**right**) as a function of temperature for compound **5** (**top**) and for compound **6** (**bottom**). In the inset of each χ_M'' graph is shown the dependence of ln (τ) versus T^{-1}. The red lines represent the fits of Arrhenius. The color lines have the same meanings as in (**left**).

The susceptibility components of both compounds also show frequency dependence, as the curves shift to lower temperatures with decreasing frequency, typical behavior of single-molecule magnets (SMMs). From the maxima of the χ_M'' curves, the thermal dependence of the relaxation time for the process was obtained, which can be determined according to the Arrhenius law, yielding effective energy barrier (U_{eff}) and pre-exponential factor (τ_0) values of 19.90 cm^{-1} and 4.19 $\times$ 10^{-9} s for **5**, and 31.1 cm^{-1} and 2.27 $\times$ 10^{-10} s for **6**, while those of the reported compound **6**·0.66EtOH·0.33H_2O are 45.9 cm^{-1} and 3.99 $\times$ 10^{-10} s. The zero-field splitting parameter (D), calculated according to $U_{eff} = |D| \cdot S^2$, is 0.76 cm^{-1} for **5** and 1.94 cm^{-1} for **6**, are similar to the values found in other hexanuclear Mn(III) compounds [13,34].

2.3. Luminescence Studies

Due to the presence of the 9-anthracenecarboxylate ligand in compounds **1**–**6**, a UV-visible study was conducted for both the free ligand and the mentioned compounds (Figure 8). The spectra were measured in ethanolic solution at a concentration of 10^{-5} M. In all compounds, the absorbance peaks of the π–π* transitions of the carboxylate ligand were observed to be slightly shifted toward red compared to the spectrum of the free ligand. The decrease in the energy of the ligand transitions is due to its coordination with Mn(III) metals [33]. The quenching effect of Mn(III) and Na+ ions (in the cases of compounds **1** and **2**) decreases the signal intensity compared to that of the free ligand [37].

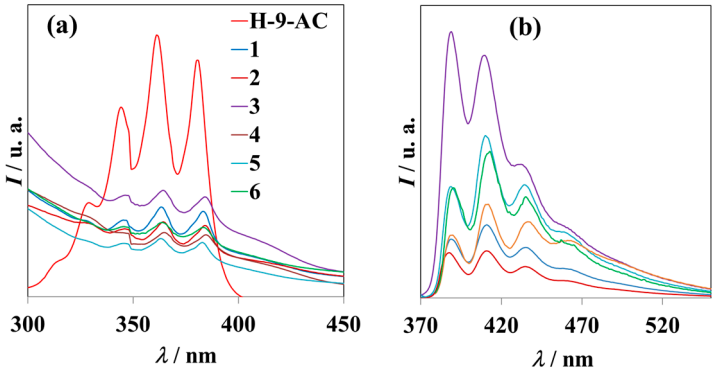


Figure 8. (**a**) Absorption of the Na(9-AC) species and of compounds **1**–**6**, and (**b**) emission spectra (λ_{em} = 364 nm) of compounds **1**–**6** in ethanol solution (10^{-5} M) measured at room temperature. Color lines have the same meanings as in (**a**).

In view of these results, the emission measurements (Figure 8), also in solution, reveal the ligand transitions under the excitation of 364 nm, centered approximately at 389 nm, 410 nm, 434 nm, and 460 nm (Figure 8b). The slight variations in the positions and relative intensities of the emission peaks are due to the different coordination modes of the 9-AC ligand in each compound [20].

3. Experimental Section

3.1. Starting Materials

$Mn(X)_2 \cdot 6H_2O$ salts (X = ClO_4^-, NO_3^-), 9-anthracenecarboxylic acid (H-9-AC)), sodium and cesium hydroxide, ethanol, tetrapropylammonium hydroxide, tetramethylammonium hydroxide, and tetrabutylammonium hydroxide were obtained from Sigma Aldrich and used without further purification.

The ligands H_2-3-Me-salox, H_2-Me-salox, and H_2-Et-salox were synthesized following the method previously described in the literature [38], employing aldehyde and EtOH as the solvents. Sodium and cesium 9-anthracenecarboxylato salts were prepared according to the synthesis previously described [39], starting from 9-anthracenecarboxylic acid and either sodium or cesium hydroxide. The syntheses of compounds **1**–**6** were conducted under aerobic conditions using the same experimental procedure, varying the anthracenecar-

boxylic salt and the ligand H_2-R-salox (A = Na^+ and R = H for **1**, A = Na^+ and R = 3-Me for **2**, A = Cs^+ and R = H for **3**, A = Cs^+ and R = 3-Me for **4**, A = Na^+ or Cs^+ and R = Me for **5** and A = Na^+ or Cs^+ and R = Et for **6**), as indicated in Scheme 4.

3.2. General Syntheses

CAUTION: Perchlorate salts of metal complexes with organic ligands are potentially explosive. Only a small amount of material should be prepared, and it should be handled with caution.

In the synthesis process, we started from an ethanolic solution of 20 mL containing 0.98 mmol of $Mn(ClO_4)_2{\cdot}6H_2O$, 0.98 mmol of the corresponding alkaline salt of anthracenecarboxylate, and the corresponding ligand H_2-R-salox. To the resulting mixture, which acquires a light brown hue, 0.5 mmols of tetrapropylammonium hydroxide, $(Pr_4N)OH$, were added. Immediately, a whitish solid precipitated and the solution darkened, turning dark green. The solution was left under agitation at room temperature for an hour and then filtered. To crystallize compounds **1**–**3**, **5**, and **6**, the slow layer diffusion method was followed, taking 10 mL of solution and 10 mL of a 1:1 mixture of diethyl ether and hexane. Two week later, dark-brown prismatic crystals were obtained. On the other hand, the crystallization of compound **4** was only possible after one month of slow evaporation of the solution. Compounds **1**–**6** can also been obtained starting from Mn(II) nitrate salt and using tetramethylammonium hydroxide or tetrabutylammonium hydroxide instead of $(Pr_4N)OH$.

The most relevant IR bands, Ref. [40], of compounds **1**–**6** are reported below:

For **1**: Selected IR bands (KBr pellet, cm^{-1}): 3435 (m, $\upsilon_{(O–H)}$), 2979-2884 (w, $\upsilon_{(–C–H)}$), 1635 (s, $\upsilon_{as(COO^-)}$), and 1601 (s, $\upsilon_{(C=N)}$).
For **2**: Selected IR bands (KBr pellet, cm^{-1}): 3444 (m, $\upsilon_{(O–H)}$), 2966-2842 (w, $\upsilon_{(–C–H)}$), 1625 (s, $\upsilon_{as(COO^-)}$), and 1589 (s, $\upsilon_{(C=N)}$).
For **3**: Selected IR bands (KBr pellet, cm^{-1}): 3416 (m, $\upsilon_{(O–H)}$), 1638 (s, $\upsilon_{as(COO^-)}$), and 1535 (m, $\upsilon_{(C=N)}$).
For **4**: Selected IR bands (KBr pellet, cm^{-1}): 3442 (m, $\upsilon_{(O–H)}$), 3028-2889 (w, $\upsilon_{(–C–H)}$), 1595 (s, $\upsilon_{as(COO^-)}$), and 1545 (s, $\upsilon_{(C=N)}$).
For **5**: Selected IR bands (KBr pellet, cm^{-1}): 3442 (m, $\upsilon_{(O–H)}$), 3050-2817 (w, $\upsilon_{(–C–H)}$), 1595 (s, $\upsilon_{as(COO^-)}$), and 1532 (s, $\upsilon_{(C=N)}$).
For **6**: Selected IR bands (KBr pellet, cm^{-1}) [a]: 3442 (m, $\upsilon_{(O–H)}$), 2986-2832 (w, $\upsilon_{(–C–H)}$), 1601 (s, $\upsilon_{as(COO^-)}$), and 1536 (s, $\upsilon_{(C=N)}$).

3.3. Physical Measurements and Magnetic Fits

Infrared spectra (4000–400 cm^{-1}) were recorded with a Perkin-Elmer 380-B spectrophotometer. The samples were prepared by mixing with KBr.

Fluorescence spectra were recorded with a Horiba Jobin Yvon SPEX Nanolog spectrophotometer at room temperature. For solid-state measurements, the samples were placed between two quartz plates.

Magnetic measurements were performed at the Mesures Magnètiques Unit from Scientific and Technological Centers (CCiTUB), Universitat de Barcelona, using a Quantum Design MPMS-XL SQUID magnetometer.

To fit the magnetic susceptibility data, the PHI program was used [41]. The error (R) associated with the divergence of the experimental values and calculations of the different fits was calculated according to the following equation:

$$R = \frac{\sum\left(\chi_M T_{exp}{}^2 - \chi_M T_{cal}{}^2\right)}{\sum \chi_M T_{exp}{}^2}$$

3.4. X-ray Crystallography

Single-crystal X-ray diffraction measurements were performed with a D8VENTURE diffractometer (Bruker) with a CMOS detector. The intensities were recorded with a graphite monochromator using Mo-Kα radiation. Lorentz polarization and absorption corrections were performed on all the samples. The structures were solved by direct methods, using the computer program SHELXS-97 [42], and refined through full matrix least squares methods, using the computer program SHELXL-2014 [43]. The SHELXLE program was used as a graphical interface. Atoms, excluding hydrogen, were located from successive difference Fourier synthesis and refined with anisotropic thermal parameters (F^2). In most cases, the hydrogen atoms were calculated, assigning the isotropic temperature factors as 1.2 or 1.5 times, with respect to bonded atoms.

CCDC numbers: 2362267 (for **1**), 2362264 (for **2**) 2362265 (for **3**), 2362266 (for **4**), 2362268 (for **5**), and 2362269 (for **6**) contain the supplementary crystallographic data for this paper. These data can be obtained free of charge via https://www.ccdc.cam.ac.uk/structures/, accessed on 12 June 2024.

4. Conclusions

In this work, six new compounds obtained from different H_2-R-salox ligands (R = H for H_2-salox; 3-CH_3 for H_2-3-Me-salox; CH_3 for H_2-Me-salox; CH_2CH_3 for H_2-Et-salox) and 9-anthracenecarboxylate anions (9-AC) have been presented. When using R-salox^{2-} ligands with hydrogen atoms coordinated to the carbon atom of the oxime group, it has been observed that the topology of the resulting compound changes depending on the presence of Na^+ or Cs^+ ions due to the different ionic radius values between these two alkali cations. Thus, from Na(9-AC), the complexes $[Mn_3NaO(salox)_3(9\text{-}AC)_2(EtOH)_3H_2O]n{\cdot}2EtOH$ (**1**·2EtOH) and $[Mn_3NaO(3\text{-}Me\text{-}salox)_3(9\text{-}AC)_2(EtOH)_3H_2O]n{\cdot}$EtOH (**2**·EtOH) have been obtained, both with chain-like structures formed by $\{Mn^{III}{}_3(\mu_3\text{-}O)(R\text{-}salox)_3\}^+$ triangles connected by hexacoordinated Na^+ cations and carboxylate anions. In contrast, when changing the cation of the carboxylic salt to Cs^+, the low-nuclearity compounds $[Mn_6O_2(salox)_6(9\text{-}AC)_2(EtOH)_2(H_2O)_2]{\cdot}3EtOH$ (**3**·3EtOH) and $[Mn_3O(3\text{-}Me\text{-}salox)_3(9\text{-}AC)(EtOH)_3(H_2O)]$ $\cdot 1.8EtOH{\cdot}3H_2O$ (**4**·1.8EtOH·3H2O) were obtained.

Using H_2-R-salox ligands with alkyl groups coordinated to the carbon atom of the oxime group, the hexanuclear compounds $[Mn_6O_2(Me\text{-}salox)_6(9\text{-}AC)_2(EtOH)_4(H_2O)_2]{\cdot}$ $0.5H_2O$ (**5**·0.5H2O) and $[Mn_6O_2(Et\text{-}salox)_6(9\text{-}AC)_2(EtOH)_4(H_2O)_2]{\cdot}3EtOH$ (**6**·3EtOH) were obtained, irrespective of whether the sodium or cesium salts of anthracenecarboxylate was used.

Compounds derived from 3-Me-salicylaldoxime, with the alkyl group bonded to the aromatic ring at an ortho position relative to the OH group, also follow the magneto-structural correlation of the compounds with $\{Mn^{III}{}_3(\mu_3\text{-}O)(R\text{-}salox)_3\}^+$ cores. Therefore, it is not only the volume of the substituent group that affects the torsion angle, but also its position relative to the oxime group bonded to Mn, as observed in other reported studies [35].

The magnetic study of compounds **1**–**6** indicates a set of antiferromagnetic interactions in compounds **1** and **2** and a combination of antiferromagnetic and ferromagnetic interactions in compounds **3**, **5**, and **6**. In all analyzed cases, the magneto-structural correlation between the intramolecular Mn^{III}-N-O-Mn^{III} torsion angle and the magnetic exchange within these units has been confirmed. For compounds **5** and **6**, magnetic measurements have revealed the slow relaxation of the magnetization, with moderate energy barriers of 19.9 and 31.1 cm^{-1}, respectively.

Absorbance and fluorescence measurements in solution show the transitions of the 9-anthracenecarboxylate chromophore for compounds **1**–**6**. Consequently, compounds **5** and **6**, with single-molecule magnets and luminescent properties, can be considered bifunctional molecular materials.

Supplementary Materials: The following supporting information can be downloaded at: https://www.mdpi.com/article/10.3390/magnetochemistry10080055/s1, Table S1: Crystallographic data for compounds **1**–**6**; Table S2: BVS parameters for the Mn ions of complexes **1**–**6**; Table S3: Distances (d, where A = acceptor atom, D = donor atom) and angles of the different hydrogen bonds observed in compounds **1**–**6**. Table S4. Data of continuous shape measures calculations of Na ions in 1 and 2 deviations from the ideal octahedron structure (ML6). Figure S1. Packing configuration observed within the unit cell of 3 showing intra- and inter-molecular hydrogen bonds (blue discontinuous line). Figure S2. Representation of hydrogen bonds (blue dashed line) in compound **4**.

Author Contributions: The manuscript was prepared from the contributions of all authors. They specifically contributed as follows: B.C.: synthesis, characterization of obtained compounds, performance of the magnetic and photoluminescence measurements, and the analysis of the results of magnetic studies for all compounds. R.V.: design and development of the general idea of the research and contribution to the original draft preparation. M.F.-B.: performance of single-crystal X-ray diffraction experiments and refinement of the crystal structure. M.S.E.F.: supervision and preparation of the final version of the manuscript. All authors have read and agreed to the published version of the manuscript.

Funding: This work was supported by the Spanish Ministry of Science and Innovation (MICINN) Project PID2023-146166NB-I00.

Data Availability Statement: The data presented in this study are available in this article or the Supplementary Materials.

Acknowledgments: The authors would like to thank Sergio Caballero and Annia Tubau for their help with the shape calculations and the revision of structure **6**, respectively.

Conflicts of Interest: There are no conflicts of interest to declare.

References

1. Milios, C.J.; Raptopoulou, C.P.; Terzis, A.; Lloret, F.; Vicente, R.; Perlepes, S.P.; Escuer, A. Hexanuclear Manganese(III) Single-Molecule Magnets. *Angew. Chem. Int. Ed.* **2004**, *43*, 210–212. [CrossRef] [PubMed]
2. Smith, A. The Structures of Phenolic Oximes and Their Complexes. *Coord. Chem. Rev.* **2003**, *241*, 61–85. [CrossRef]
3. Afrati, T.; Dendrinou-Samara, C.; Raptopoulou, C.; Terzis, A.; Tangoulis, V.; Tsipis, A.; Kessissoglou, D.P. Experimental and Theoretical Study of the Antisymmetric Magnetic Behavior of Copper *Inverse* -9-Metallacrown-3 Compounds. *Inorg. Chem.* **2008**, *47*, 7545–7555. [CrossRef] [PubMed]
4. Stamatatos, T.C.; Dionyssopoulou, S.; Efthymiou, G.; Kyritsis, P.; Raptopoulou, C.P.; Terzis, A.; Vicente, R.; Escuer, A.; Perlepes, S.P. The First Cobalt Metallacrowns: Preparation and Characterization of Mixed-Valence Cobalt(II/III), Inverse 12-Metallacrown-4 Complexes. *Inorg. Chem.* **2005**, *44*, 3374–3376. [CrossRef] [PubMed]
5. Stemmler, A.J.; Kampf, J.W.; Pecoraro, V.L. Synthesis and Crystal Structure of the First Inverse 12-Metallacrown-4. *Inorg. Chem.* **1995**, *34*, 2271–2272. [CrossRef]
6. Vlahopoulou, G.; Escuer, A.; Font-Bardia, M.; Calvet, T. Synthesis and Characterization of Co^{III}_3 Inverse Metallacrowns via Use of 6-Methyl-2-Pyridylaldoxime. *Inorg. Chem. Commun.* **2012**, *16*, 78–80. [CrossRef]
7. Flamourakis, A.G.; Kalofolias, D.A.; Siczek, M.; Lis, T.; Brechin, E.K.; Milios, C.J. New Members of the [Mn_6/Oxime] Family and Analogues with Converging [Mn_3] Planes. *J. Coord. Chem.* **2016**, *69*, 826–840. [CrossRef]
8. Perivolaris, A.; Fidelli, A.M.; Inglis, R.; Kessler, V.G.; Slawin, A.M.Z.; Brechin, E.K.; Papaefstathiou, G.S. A Family of Hexanuclear Mn(III) Single-Molecule Magnets. *J. Coord. Chem.* **2014**, *67*, 3972–3986. [CrossRef]
9. Hołyńska, M.; Dehnen, S. A Series of [Mn_6] Complexes with Terminal Functional Groups. *Z. Anorg. Allg. Chem.* **2012**, *638*, 763–769. [CrossRef]
10. Inglis, R.; Jones, L.F.; Milios, C.J.; Datta, S.; Collins, A.; Parsons, S.; Wernsdorfer, W.; Hill, S.; Perlepes, S.P.; Piligkos, S.; et al. Attempting to Understand (and Control) the Relationship between Structure and Magnetism in an Extended Family of Mn_6 Single-Molecule Magnets. *Dalton Trans.* **2009**, 3403–3412. [CrossRef]
11. Milios, C.J.; Vinslava, A.; Wernsdorfer, W.; Prescimone, A.; Wood, P.A.; Parsons, S.; Perlepes, S.P.; Christou, G.; Brechin, E.K. Spin Switching via Targeted Structural Distortion. *J. Am. Chem. Soc.* **2007**, *129*, 6547–6561. [CrossRef] [PubMed]
12. Chaudhuri, P. Homo- and Hetero-Polymetallic Exchange Coupled Metal-Oximates. *Coord. Chem. Rev.* **2003**, *243*, 143–190. [CrossRef]
13. Milios, C.J.; Inglis, R.; Vinslava, A.; Bagai, R.; Wernsdorfer, W.; Parsons, S.; Perlepes, S.P.; Christou, G.; Brechin, E.K. Toward a Magnetostructural Correlation for a Family of Mn_6 SMMs. *J. Am. Chem. Soc.* **2007**, *129*, 12505–12511. [CrossRef] [PubMed]
14. Milios, C.J.; Vinslava, A.; Wernsdorfer, W.; Moggach, S.; Parsons, S.; Perlepes, S.P.; Christou, G.; Brechin, E.K. A Record Anisotropy Barrier for a Single-Molecule Magnet. *J. Am. Chem. Soc.* **2007**, *129*, 2754–2755. [CrossRef]

15. Inglis, R.; Jones, L.F.; Mason, K.; Collins, A.; Moggach, S.A.; Parsons, S.; Perlepes, S.P.; Wernsdorfer, W.; Brechin, E.K. Ground Spin State Changes and 3 D Networks of Exchange Coupled [Mn^{III}_3] Single-Molecule Magnets. *Chem.—A Eur. J.* **2008**, *14*, 9117–9121. [CrossRef] [PubMed]
16. Song, X.; Liu, R.; Zhang, S.; Li, L. A Rare Ferromagnetic Manganese(III) Hexanuclear Cluster. *Inorg. Chem. Commun.* **2010**, *13*, 828–830. [CrossRef]
17. An, G.-Y.; Cui, A.-L.; Kou, H.-Z. Assembly of Oximate-Bridged Mn_6 Cluster to a One-Dimensional Chain. *Inorg. Chem. Commun.* **2011**, *14*, 1475–1478. [CrossRef]
18. Haryono, M.; Kalisz, M.; Sibille, R.; Lescouëzec, R.; Fave, C.; Trippe-Allard, G.; Li, Y.; Seuleiman, M.; Rousselière, H.; Balkhy, A.M.; et al. One Dimensional Assembly of Mn6 Single Molecule Magnets Linked by Oligothiophene Bridges. *Dalton Trans.* **2010**, *39*, 4751–4756. [CrossRef] [PubMed]
19. Schwarz, F.P.; Wasik, S.P. Fluorescence Measurements of Benzene, Naphthalene, Anthracene, Pyrene, Fluoranthene, and Benzo[e]Pyrene in Water. *Anal. Chem.* **1976**, *48*, 524–528. [CrossRef]
20. Li, L.; Hu, T.-L.; Li, J.-R.; Wang, D.-Z.; Zeng, Y.-F.; Bu, X.-H. Metal–Organic Coordination Architectures of 9,10-Bis(N-Benzimidazolyl)Anthracene: Syntheses, Structures and Emission Properties. *CrystEngComm* **2007**, *9*, 412–420. [CrossRef]
21. Alaimo, A.A.; Takahashi, D.; Cunha-Silva, L.; Christou, G.; Stamatatos, T.C. Emissive {Mn_4^{III} Ca} Clusters with Square Pyramidal Topologies: Syntheses and Structural, Spectroscopic, and Physicochemical Characterization. *Inorg. Chem.* **2015**, *54*, 2137–2151. [CrossRef] [PubMed]
22. Beedle, C.C.; Stephenson, C.J.; Heroux, K.J.; Wernsdorfer, W.; Hendrickson, D.N. Photoluminescent Mn_4 Single-Molecule Magnet. *Inorg. Chem.* **2008**, *47*, 10798–10800. [CrossRef] [PubMed]
23. Alexandropoulos, D.I.; Mowson, A.M.; Pilkington, M.; Bekiari, V.; Christou, G.; Stamatatos, T.C. Emissive Molecular Nanomagnets: Introducing Optical Properties in Triangular Oximato {Mn^{III}_3} SMMs from the Deliberate Replacement of Simple Carboxylate Ligands with Their Fluorescent Analogues. *Dalton Trans.* **2014**, *43*, 1965–1969. [CrossRef]
24. Kalofolias, D.A.; Flamourakis, A.G.; Siczek, M.; Lis, T.; Milios, C.J. A Bulky Oxime for the Synthesis of Mn(III) Clusters. *J. Coord. Chem.* **2015**, *68*, 3472–3484. [CrossRef]
25. Manoli, M.; Inglis, R.; Piligkos, S.; Yanhua, L.; Wernsdorfer, W.; Brechin, E.K.; Tasiopoulos, A.J. A Hexameric [$Mn^{III}_{18}Na_6$] Wheel Based on [$Mn^{III}_3O]^{7+}$ Sub-Units. *Chem. Commun.* **2016**, *52*, 12829–12832. [CrossRef] [PubMed]
26. Raptopoulou, C.P.; Boudalis, A.K.; Lazarou, K.N.; Psycharis, V.; Panopoulos, N.; Fardis, M.; Diamantopoulos, G.; Tuchagues, J.-P.; Mari, A.; Papavassiliou, G. Salicylaldoxime in Manganese(III) Carboxylate Chemistry: Synthesis, Structural Characterization and Physical Studies of Hexanuclear and Polymeric Complexes. *Polyhedron* **2008**, *27*, 3575–3586. [CrossRef]
27. Yang, C.-I.; Feng, P.-Y.; Chen, Y.-T.; Tsai, Y.-J.; Lee, G.-H.; Tsai, H.-L. Molecular Architecture Based on Manganese Triangles: Monomer, Dimer, and One-Dimensional Polymer. *Polyhedron* **2011**, *30*, 3265–3271. [CrossRef]
28. Geng, J.-P.; Wang, Z.-X.; He, X.; Xiao, H.-P.; Li, M.-X. A Novel 2D Coordination Polymer Based on Triangular-Shaped [Mn_3O] Units Bridged by Sodium Ions and Benzene-1,2,4,5-Tetracarboxylate. *Inorg. Chem. Commun.* **2011**, *14*, 997–1000. [CrossRef]
29. Wu, L.-F.; Wang, Z.-X.; Geng, J.-P.; Xiao, H.-P.; Li, M.-X. A Two-Dimensional Coordination Polymer Constructed from Hexanuclear Manganese Units with Sodium Ions as Auxiliary Bridges. *Inorg. Chim. Acta* **2014**, *412*, 1–5. [CrossRef]
30. Mukherjee, S.; Mukherjee, P.S. Role of Dicarboxylate Linkers in Mn^{III} -Salicylaldoximate Based Extended Structures: Synthesis, Structures, and Magnetic Behavior. *Chem.—A Eur. J.* **2013**, *19*, 17064–17074. [CrossRef]
31. Brown, I.D.; Altermatt, D. Bond-Valence Parameters Obtained from a Systematic Analysis of the Inorganic Crystal Structure Database. *Acta Crystallogr. B* **1985**, *41*, 244–247. [CrossRef]
32. ALVAREZ, S.; ALEMANY, P.; CASANOVA, D.; CIRERA, J.; LLUNELL, M.; AVNIR, D. Shape Maps and Polyhedral Interconversion Paths in Transition Metal Chemistry. *Coord. Chem. Rev.* **2005**, *249*, 1693–1708. [CrossRef]
33. Jones, L.F.; Cochrane, M.E.; Koivisto, B.D.; Leigh, D.A.; Perlepes, S.P.; Wernsdorfer, W.; Brechin, E.K. Tuning Magnetic Properties Using Targeted Structural Distortion: New Additions to a Family of Mn_6 Single-Molecule Magnets. *Inorg. Chim. Acta* **2008**, *361*, 3420–3426. [CrossRef]
34. Escuer, A.; Cordero, B.; Font-Bardia, M.; Teat, S.J.; Roubeau, O. Manganese–Salicyloximate Clusters Starting from [Mn^{II} $(Hfacac)_2$]: From Mn_4 to Mn_{12}. *Eur. J. Inorg. Chem.* **2016**, *2016*, 1232–1241. [CrossRef]
35. Milios, C.J.; Vinslava, A.; Whittaker, A.G.; Parsons, S.; Wernsdorfer, W.; Christou, G.; Perlepes, S.P.; Brechin, E.K. Microwave-Assisted Synthesis of a Hexanuclear Mn^{III} Single-Molecule Magnet. *Inorg. Chem.* **2006**, *45*, 5272–5274. [CrossRef] [PubMed]
36. Tarushi, A.; Hatzidimitriou, A.G.; Estrader, M.; Kessissoglou, D.P.; Tangoulis, V.; Psomas, G. Toward Multifunctional Materials Incorporating Stepladder Manganese(III) Inverse-[9-MC-3]-Metallacrowns and Anti-Inflammatory Drugs. *Inorg. Chem.* **2017**, *56*, 7048–7057. [CrossRef] [PubMed]
37. Fleischauer, P.D.; Fleischauer, P. Photoluminescence of Transition Metal Coordination Compounds. *Chem. Rev.* **1970**, *70*, 199–230. [CrossRef]
38. Dunstan, W.R.; Henry, T.A. VIII.—Occurrence of Orthohydroxyacetophenone in the Volatile Oil of Chione Glabra. *J. Chem. Soc. Trans.* **1899**, *75*, 66–71. [CrossRef]
39. Ueno, A.; Moriwaki, F.; Osa, T.; Hamada, F.; Murai, K. Association, Photodimerization, and Induced-Fit Types of Host-Guest Complexation of Anthracene-Appended .Gamma.-Cyclodextrin Derivatives. *J. Am. Chem. Soc.* **1988**, *110*, 4323–4328. [CrossRef]
40. Nakamoto, K. *Infrared and Raman Spectra of Inorganic and Coordination Compounds*; Wiley: Hoboken, NJ, USA, 2008; ISBN 9780471743392.

41. Chilton, N.F.; Anderson, R.P.; Turner, L.D.; Soncini, A.; Murray, K.S. PHI: A Powerful New Program for the Analysis of Anisotropic Monomeric and Exchange-coupled Polynuclear *d* - and *f* -block Complexes. *J. Comput. Chem.* **2013**, *34*, 1164–1175. [CrossRef]
42. Sheldrick, G.M. A Short History of *SHELX*. *Acta Crystallogr. A* **2008**, *64*, 112–122. [CrossRef] [PubMed]
43. Sheldrick, G.M. Crystal Structure Refinement with *SHELXL*. *Acta Crystallogr. C Struct. Chem.* **2015**, *71*, 3–8. [CrossRef] [PubMed]

Disclaimer/Publisher's Note: The statements, opinions and data contained in all publications are solely those of the individual author(s) and contributor(s) and not of MDPI and/or the editor(s). MDPI and/or the editor(s) disclaim responsibility for any injury to people or property resulting from any ideas, methods, instructions or products referred to in the content.